RESEARCH ARTICLE

ADVANCED OPTICAL MATERIALS
www.advopticalmat.de

Dual Multiresonance Core Strategy Enable Efficient Pure Blue Organic Light-Emitting Devices Based on Fluorene Linkages

Xiangan Song, Shaogang Shen, Binghong He, Shengnan Zou, Aliaksei A. Vaitusionak, Sergei V. Kostjuk, Yafei Wang, Ying Wang,* and Yong Zhang**

Multiresonance thermally activated delayed fluorescence (MR-TADF) emitters with high color purity in virtue of their inherent narrowband emission have received great interest in organic light-emitting diodes (OLEDs). However, it remains a big challenge to develop the ultrapure blue MR-TADF emitters with high efficiency. In this work, a novel "dual-MR-core" strategy is proposed by connecting two parent N-B-O-skeletons with non-conjugate 9-position substituted fluorene linkages for high efficient deep-blue MR-TADF emitters, namely H-FOBN and Me-FOBN, which possess the highly twisted structure with suppressed aggregation. Finally, the vacuum-deposited deep-blue OLED exhibits excellent external quantum efficiency (EQE) of 25.1% with small full width at half maximum (FWHM) of 28 nm, as well as CIE of (0.14, 0.08). Furthermore, owing to enhanced solubility, the solution-processed deep-blue OLED based on Me-FOBN shows EQE of 11.3%, with small FWHM of 32 nm and CIE of (0.14,0.09). These outstanding performances confirm that this "dual-MR-core" strategy provides a feasible approach to develop high efficient ultrapure blue MR-TADF emitters.

1. Introduction

Organic light-emitting diodes (OLEDs) have been considered as a promising candidate in the field of panel display, relying on its superior advantages of flexible characteristics and high display quality.[1–4] Recently, thermally activated delayed fluorescence (TADF) emitters have been extensively studied owing to their nearly 100% internal quantum efficiency (IQE) which is enabled by converting triplet excitons to radiative single excitons through reverse intersystem crossing (RISC) process acquired from minimized energy gap (ΔE_{ST}) between the lowest triplet (T_1) and singlet excited states (S_1).[5–9] Generally, this requirement can be realized by separating the highest occupied molecular orbital (HOMO) and the lowest unoccupied molecular orbital (LUMO) via a twist donor–acceptor (D–A) molecular structure.[10–15] In the past few years, many reported OLEDs employing TADF emitters with D–A molecular structure exhibit external quantum efficiency (EQE) exceeding 30%.[16–18] Despite the success of D–A molecular structure, their intrinsic structural relaxation between the ground state and excited state will inevitably lead to broad emission band and therefore a poor color purity, limiting their further applications in the field of larger color gamut.[19,20] In addition, their inherent long-range charge transfer (LRCT) character will result in bathochromic shifted emission which can be further aggravated by intermolecular interactions, generating great challenges to obtain highly efficient deep-blue TADF emitters.[21] Consequently, a novel molecular design strategy of TADF emitters is thus highly needed to be designed toward higher color purity, especially for pure deep-blue emission ($CIE_y < 0.10$).

Recently, to meet the requirements of high color purity, a new TADF molecular structure with multi-resonance (MR) effect has been developed based on rigid polycyclic aromatic frameworks composed of electron-deficient atom (boron, B) and electron-rich atom (nitrogen, N), giving opposite electronic effect of short-range charge transfer (SRCT) to realize well-separated distributions of frontier molecular orbitals (FMOs) and therefore a small ΔE_{ST}.[22–26] Their inherent rigid molecular can suppress structural relaxation and the dominant non-bonding character can

X. Song, S. Zou, Y. Zhang
School of Materials Science and Engineering
Harbin Institute of Technology
Harbin 150001, China
E-mail: yongzhang@hit.edu.cn

S. Shen, Y. Wang
Key Laboratory of Photochemical Conversion and Optoelectronic Materials
and TIPC-CityU Joint Laboratory of Functional Materials and Device
Technical Institute of Physics and Chemistry
Chinese Academy of Sciences
Beijing 100190, China
E-mail: wangy@mail.ipc.ac.cn

B. He, Y. Wang
School of Materials Science & Engineering
Changzhou University
Changzhou 213164, P. R. China

A. A. Vaitusionak, S. V. Kostjuk
Research Institute for Physical Chemical Problems
Belarusian State University
Minsk 220006, Belarus
E-mail: kostjuks@bsu.by

The ORCID identification number(s) for the author(s) of this article can be found under https://doi.org/10.1002/adom.202401505

DOI: 10.1002/adom.202401505

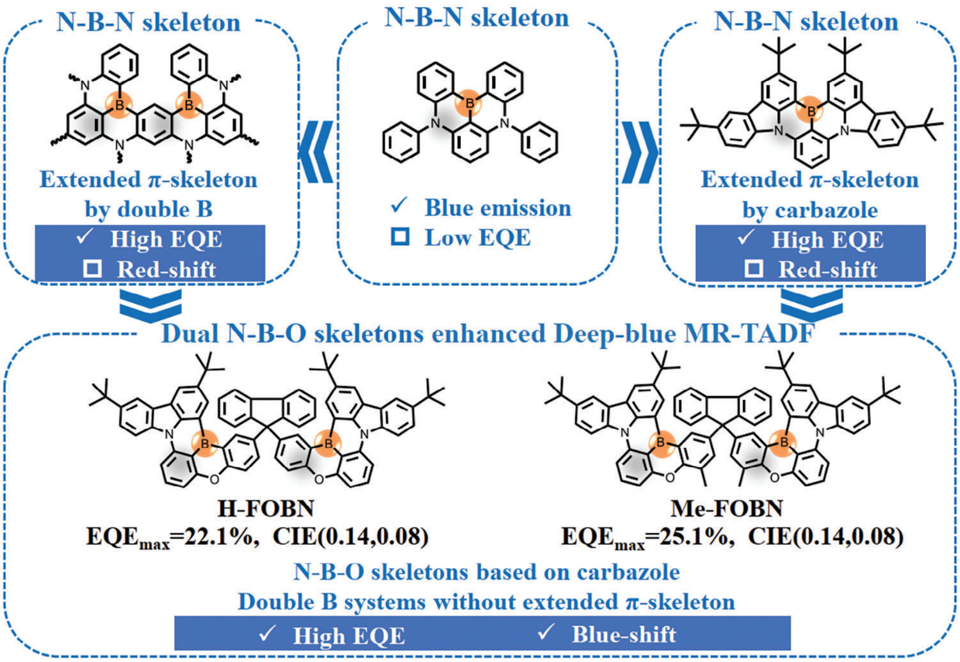

Figure 1. Molecular design strategies and the summary performances of H-FOBN and Me-FOBN.

minimize the energy gaps between the vibrational energy levels, leading to narrowband emission.[27–29] Currently, one of the most challenging problems in OLED is to establish rationale molecular design strategies toward deep-blue MR-TADF emitters ($\mathrm{CIE}_y < 0.10$) together with high efficiency.[30] For example, the well-known blue MR-TADF emitter DABNA-1 based on N-B-N-skeleton display emission peak at 459 nm and full width at half maximum (FWHM) of 28 nm with CIE of (0.13, 0.09). However, the OLED based on DABNA-1 displays unsatisfactory EQE of only 13.5%.[31] To enhance efficiency, the diphenylamine in DABNA-1 was replaced by 3,6-di-*tert*-butylcarbazole to synthesize the extended π-conjugated skeleton tCzBN (aka. DtBuCzB or BBCz-SB), which exhibited the improved EQE over 20%. However, the serious red-shifted emissions were observed with CIE_y values over 0.40.[32,33] Another extended π-conjugated strategy is to introduce double B atoms into MR-skeletons and then the enhanced OLED performances were able to be obtained, but most of them accompanied with the red-shifted emission, resulting in CIE_y values over 0.10.[28,34,35] In addition, these emitters also suffer severe molecular aggregation due to the inherent planar structures, which also leads to the poor solubility and limited applications in the solution-processed OLEDs.[34,36,37] It thus becomes highly desirable to develop the molecular design strategy for narrowband blue MR-TADF emitters, which can achieve high efficiency and maintain deep-blue emission with $\mathrm{CIE}_y < 0.10$ simultaneously.

Herein, we proposed a novel “dual-MR-core” molecular design strategy and prepared two blue MR-TADF emitters, namely H-FOBN and Me-FOBN, which were connected two N-B-O-skeletons with 9-position substituted fluorene linkages (**Figure 1**). The N-B-O-skeletons has a weakened electron donating character with oxygen substitutes, which will induce a blue-shift emission compared with the B–N only emitters. In addition, unlike the extended coplanar π-conjugated double-B MR-TADF emitters, the non-conjugated connection in H-FOBN and Me-FOBN emitters can make the N-B-O cores emit independently, providing the inhibited bathochromic shift and high EQE simultaneously. Furthermore, the highly twisted structure with 9-position substituted fluorene linkages can suppress molecular aggregation and improve the solubility, giving solution processability. Consequently, the vacuum-deposited OLED based on Me-FOBN exhibited high color purity with small FWHM of 28 nm and CIE of (0.14,0.08), and the excellent EQE of 25.1%. In addition, the solution-processed OLED based on Me-FOBN shows EQE of 11.3% with small FWHM of 32 nm and CIE of (0.14,0.09). These outstanding performances of vacuum-deposited and solution-processed devices based on H-FOBN and Me-FOBN confirm the effectiveness of this molecular design strategy.

2. Results and Discussion

The 9-position substituted fluorene units were used as linkage to synthesize the target double-B emitters H-FOBN and Me-FOBN by one-step cascade lithiation-borylation-annulation reactions, and the details were shown in Supporting Information. It is noted that both H-FOBN and Me-FOBN have good solubilities in common organic solvents, indicating their promising potential in solution-processed OLEDs. The nuclear magnetic resonance (NMR) and matrix-assisted laser desorption ionization time-of-flight (MALDI-TOF) spectroscopy were further employed to confirm the molecular structures of H-FOBN and Me-FOBN (Figures S9–S14, Supporting Information). In addition, as shown in Figure S1 (Supporting Information), the decomposition temperatures (T_d) obtained from thermogravimetric analysis (TGA) were as high as 501 °C and 504 °C for H-FOBN and Me-FOBN,

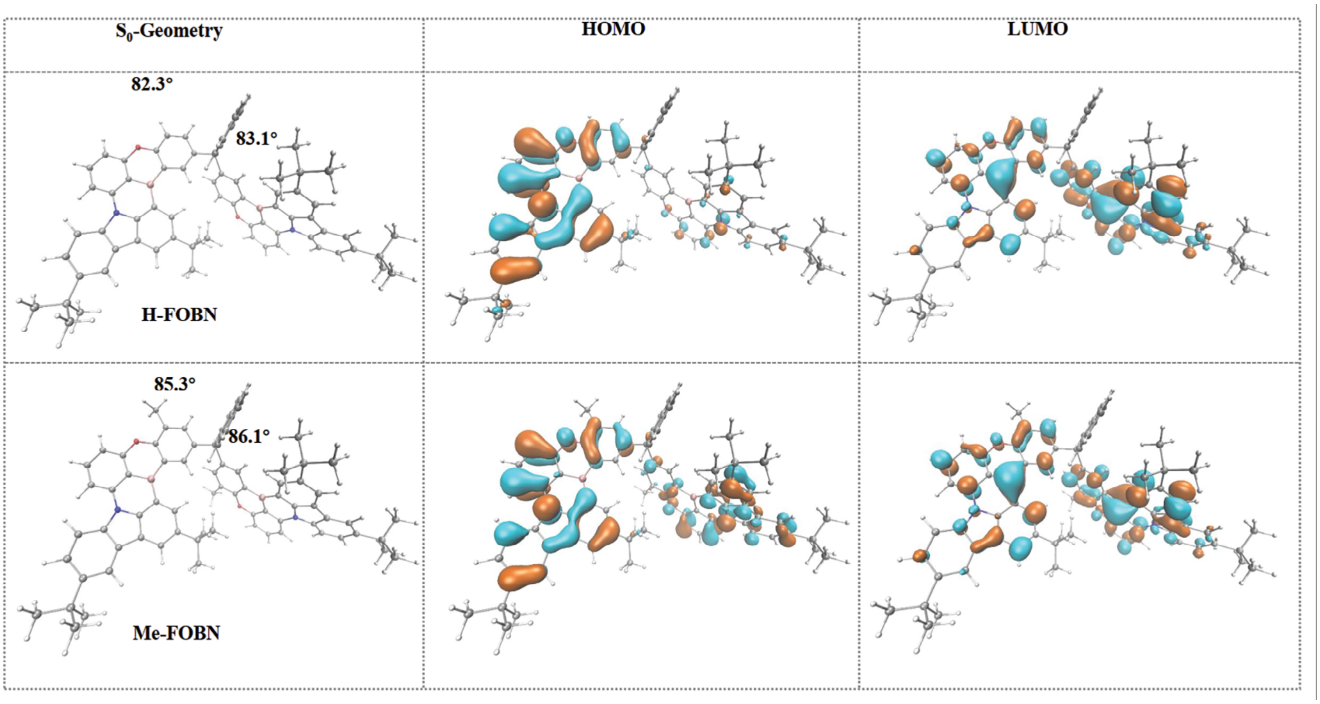

Figure 2. S_0 geometries and FMOs distributions of H-FOBN and Me-FOBN.

respectively, confirming the good thermal stabilities for OLED fabrication through vacuum thermal deposition. To explore the electrochemical properties, the cyclic voltammetry (CV) was used to measure the oxidation potentials of H-FOBN and Me-FOBN. The HOMO energy levels were calculated to be as −5.77 and −5.74 eV, respectively. Furthermore, the LUMO energy levels of H-FOBN and Me-FOBN were obtained as −3.03 and −2.99 eV from optical bandgaps (E_g) and HOMO levels. The DFT calculated HOMOs of H-FOBN and Me-FOBN are 5.40 and 5.30 eV, and the LUMOs are 1.90 and 1.80 eV respectively. The slightly high-lying HOMO and LUMO energy levels in Me-FOBN are attributed to that the electron-donating of methyl group which enhance the electron-donating capability of nitrogen atoms and weaken the electron-withdrawing capability of boron atoms simultaneously.

The S_0 geometries and frontier molecular orbitals (FMOs) distributions of H-FOBN and Me-FOBN were investigated by density function theory (DFT). As shown in **Figure 2**, the S_0 geometries of H-FOBN and Me-FOBN exhibit highly twisted structure with 9-position substituted fluorene linkages, which weaken the intermolecular aggregation and increase the solubility. The dihedral angles between fluorene and N-B-O-skeletons are 82.3° and 81.3° for H-FOBN and 85.3° and 86.1° for Me-FOBN, respectively. The FMOs distributions of H-FOBN and Me-FOBN show typical MR character and are on N-B-O-skeletons, implying that the two parent MR cores participate in emission which will increase the quantum efficiencies. Furthermore, no FMOs distributions are observed on the non-conjugate 9-position substituted fluorene linkages, which can induce each MR core to emit independently and then avoid the bathochromic shift resulted from the extended π-conjugation. In addition, the FMOs distributions of Me-FOBN on two parent MR cores are more uniform than that of H-FOBN. To clarify the excitation characters of S_1 states of H-FOBN and Me-FOBN, the hole–electron analysis was used to calculate the hole and electron distributions.[38] As shown in Figure S3 (Supporting Information), the hole and electron distribute on both core 1 and 2, and exhibit obvious overlap on both core 1 and 2, generating dual-MR-core-emission character. As a result, the molecular structures of H-FOBN and Me-FOBN with the 9-position substituted fluorene linkages exhibit obvious dual-MR-core-emission characters, indicating their potential in highly efficient deep-blue OLEDs.

To clarify the photophysical properties of H-FOBN and Me-FOBN, the UV/Vis absorption, photoluminescence (PL) and phosphorescence (Ph) spectra were measured. As shown in **Figure 3a** and **Table 1**, the absorption spectra of H-FOBN and Me-FOBN in toluene show narrow absorption bands with peaks at 437 and 436 nm, respectively, which belong to the intramolecular charge transfer of MR effect. The optical E_gs of H-FOBN and Me-FOBN were calculated to be 2.74 and 2.75 eV, respectively, and the slightly higher E_g of Me-FOBN is consistent with its blue-shifted emission. Remarkably, the PL spectra of H-FOBN and Me-FOBN in toluene present deep-blue narrowband emission with peaks at 455 and 454 nm, respectively. The Stokes shift of H-FOBN and Me-FOBN were as small as 18 nm, which should be ascribed to the suppressed molecular structural relaxation. Therefore, ultra-pure blue emissions with FWHM of 21 and 20 nm were obtained for H-FOBN and Me-FOBN, respectively. From the onsets of PL and Ph spectra at 77 K, the S_1/T_1 energy levels of H-FOBN and Me-FOBN can be obtained as 2.78 eV/2.62 eV and 2.79 eV/2.65 eV, respectively, resulting in small ΔE_{ST} of 0.16 eV and 0.14 eV. The smaller ΔE_{ST} of Me-FOBN will be able to lead to more efficient RISC process. Furthermore, as shown in Figure S4 and Table S1 (Supporting Information),

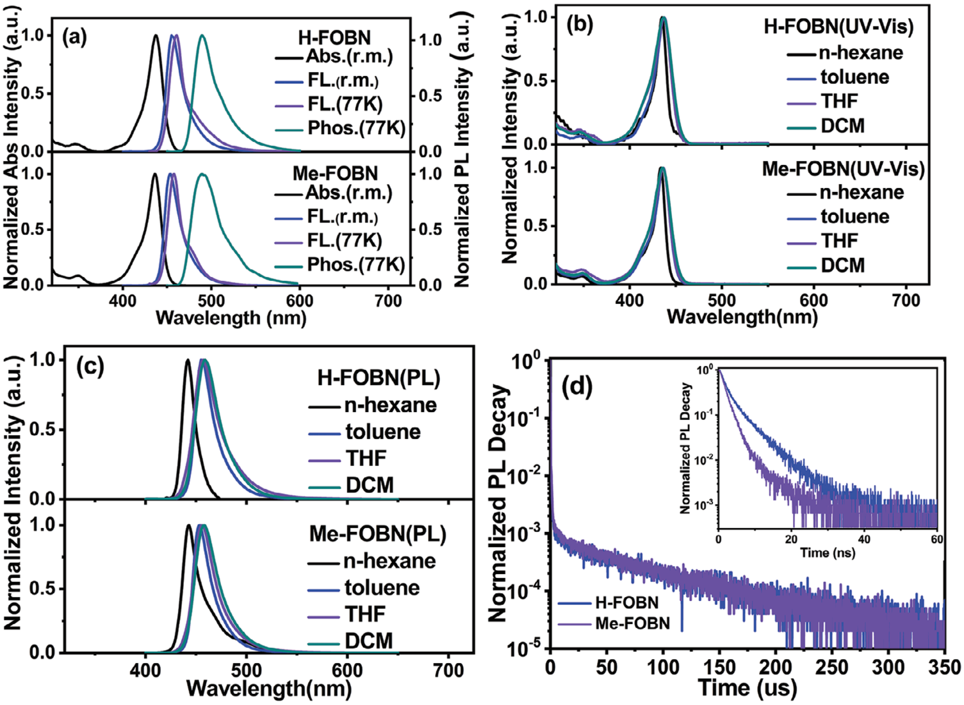

Figure 3. a) UV–visible absorption, photoluminescence spectra and phosphorescence spectra of H-FOBN and Me-FOBN in toluene (1×10^{-5} M) b) UV–visible absorption and c) fluorescence spectra (measured at 300 K) in various solutions (n-hexane, toluene, THF and DCM). d) Transient photoluminescence decay curves of 1 wt% of H-FOBN and Me-FOBN in 26DCzPPy under vacuum condition (inset: prompt decay curves).

the PL spectra of H-FOBN and Me-FOBN in doping films (from 1 wt% to 20 wt% in 26DCzPPy) were also tested. With the increase of the doping concentration from 1 to 20 wt%, the PL spectra of H-FOBN and Me-FOBN display small bathochromic shift of 13 and 10 nm, and the spectra broadening is only around 3 nm compared to that in solution, confirming the suppressed intermolecular aggregation from the highly twisted 9-position substituted fluorene structure. In addition, the PL spectra of Me-FOBN presents less-sensitive to the doping concentration owing to the additional two methyl substitutes which will enhance steric hindrance and further decrease intermolecular interaction. Simultaneously, in order to elucidate solvatochromism of H-FOBN and Me-FOBN, the absorption and PL spectra in various solvents (*n*-hexane, toluene, tetrahydrogen furan (THF) and dichloromethane (DCM)) were measured. As shown in Figure 3b and Table S2 (Supporting Information), almost no changes in the absorption bands of H-FOBN and Me-FOBN from n-hexane to DCM were observed. From Figure 3c, with the increase of the polarity, the PL spectra of H-FOBN and Me-FOBN exhibit very small bathochromic shift of 17 and 15 nm, and also very small spectra broadening, indicating negligible solvatochromic effect. These results, in combination with theoretical calculations, indicate that the dual-MR-core molecular structure with 9-position substituted fluorene linkage in H-FOBN and Me-FOBN emitter remain the SRCT character.

The TADF characters of H-FOBN and Me-FOBN were further investigated. As shown in Figure S5 (Supporting Information), the PL spectra of H-FOBN and Me-FOBN in toluene under N_2 show much stronger fluorescence intensity than that under O_2, which is typical for TADF emitters. The photoluminescence quantum yields (PLQYs) of H-FOBN and Me-FOBN in 1 wt% doping films under vacuum were measured as 82% and 86%, respectively. Due to the quenched triplet excitons by O_2, the PLQYs measured under air were decreased to be 70% and 72%, respectively, indicating the typical TADF characters of H-FOBN and Me-FOBN. Remarkably, Me-FOBN displays slightly higher PLQY due to the slight stronger suppressed intermolecular aggregation and more efficient RISC process compared to that of H-FOBN. Furthermore, the time-resolved photoluminescence (TRPL) spectra of H-FOBN and Me-FOBN in 1 wt% doping films were also measured. As shown in Figure 3d, the biexponential decay curves were observed with two components composed of prompt and delayed emission. The prompt lifetimes of H-FOBN and Me-FOBN are obtained to be 4.5 ns and 2.3 ns while

Table 1. Summary of photophysical data of H-FOBN and Me-FOBN.

Emitter	λ_{abs} [nm]	λ_{PL} [nm]	Stoke shift [nm]	E_{S1}/E_{T1} [eV]	ΔE_{ST} [eV]	PLQY [%]	FWHM [nm]	τ_p[ns]/τ_d[µs]	k_{RISC} [$\times10^4$ s^{-1}]
H-FOBN	437	455	18	2.78/2.62	0.16	82	21	4.5/75.6	6.4
Me-FOBN	436	454	18	2.79/2.65	0.14	86	20	2.3/67.2	7.5

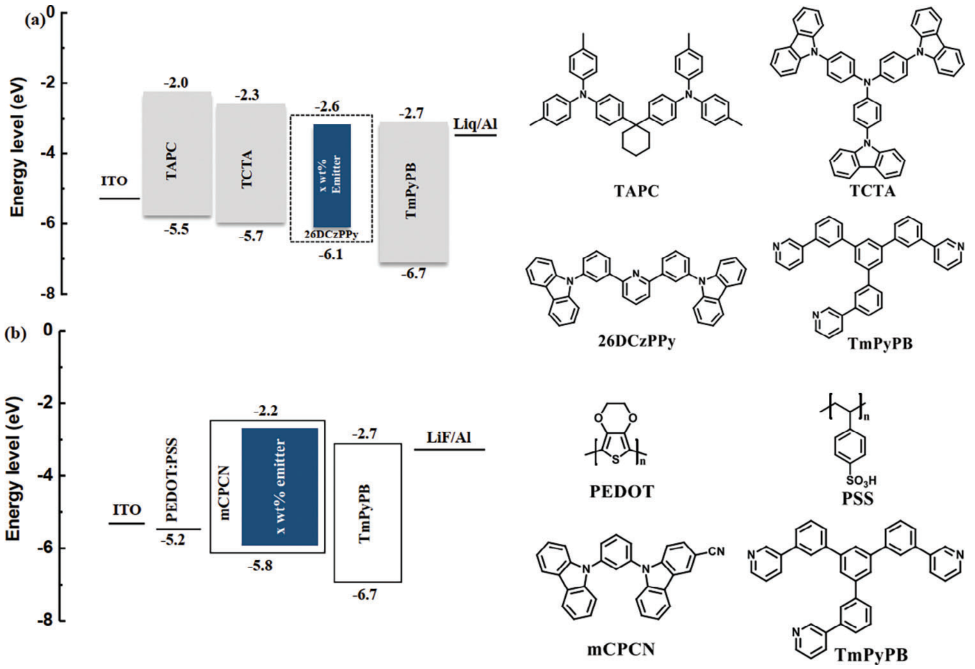

Figure 4. The device structure of a) vacuum and b) solution- processible.

the delayed lifetimes are 75.6 and 67.2 µs, respectively. Significantly, the decreased delayed components of two emitters under air atmosphere further illustrate their TADF characters (Figure S6, Supporting Information). In addition, the H-FOBN and Me-FOBN show promising k_{RISC} of 6.4×10^4 s^{-1} and 7.5×10^4 s^{-1}, respectively, acquired from efficient utilization of triplet excitons by dual-core molecular structure. Remarkably, the slightly higher k_{RISC} of Me-FOBN originates from its smaller ΔE_{ST}, implying smaller efficiency roll-off in OLEDs. As a result, the dual-MR-core molecular structure of H-FOBN and Me-FOBN with 9-position substituted fluorene linkages present the significant TADF effect, which are promising to generate ultrapure blue OLEDs with high efficiency.

To examine the electroluminescent performance of H-FOBN and Me-FOBN emitters, vacuum-deposited and solution-processed OLED devices were fabricated, and the device structure and the chemical structure of each layer were shown in **Figure** 4. The device performances based on H-FOBN and Me-FOBN emitters are summarized in **Table** 2 and Tables S3 and S4 (Supporting Information). **Figure** 5a,b shows the L-EQE curves and EL spectra of vacuum-deposited OLEDs. It can see that both H-FOBN and Me-FOBN devices exhibit pure blue narrowband emission benefiting from their inherent MR effect. At the doping concentration of 1 wt%, the pure blue EL emission peaks of H-FOBN and Me-FOBN devices are at 456 nm and 456 nm with small FWHM of 30 nm and 28 nm, respectively, and their corresponding CIE coordinates are (0.14,0.08) and (0.14,0.08). When the doping concentration is increased from 1 to 10 wt%, the EL spectra of H-FOBN and Me-FOBN devices exhibit very little bathochromic shifting and spectra broadening, originating from the negligible intermolecular aggregation. The different emission bands between doped film and vacuum-deposited device may be caused by the different energy transfer mechanisms under photoexcitation and electroexcitation conditions H-FOBN device exhibit the best EQE of 22.1% at 1 wt% doping concentration with the current efficiency (CE) and brightness of 22.0 cd A^{-1} and 3370 cd m^{-2}, respectively. Meanwhile, Me-FOBN device gave the best EQE of 25.1% with the CE and brightness of 28.7 cd A^{-1} and 3560 cd m^{-2}, respectively, which is consistent with its high PLQY. Especially, at various doping concentrations, Me-FOBN-based OLEDs exhibit better performances than that of H-FOBN, which is attributed to the enhanced k_{RISC} and suppressed

Table 2. Summary of OLED device performance of H-FOBN and Me-FOBN.

Emitter	λ_{EL}[c] [nm]	FWHM[d] [nm]	V_{on}[e] [eV]	L_{max}[f] [cd m^{-2}]	CE[g] [cd A^{-1}]	EQE[h] [%]	CIE[i]
H-FOBN[a]	456	30	5.0	3370	22.0	22.1	(0.14,0.08)
Me-FOBN[a]	456	28	4.7	3560	28.7	25.1	(0.14,0.08)
H-FOBN[b]	460	32	5.0	415	8.1	9.2	(0.14,0.10)
Me-FOBN[b]	458	32	5.0	312	9.3	11.3	(0.14,0.09)

[a] Vacuum-deposited OLED at doping ratio of 1 wt%; [b] Solution-processed OLED at doping ratio of 1 wt%; [c] Electroluminescence peak wavelength; [d] Full width at half maximum; [e] Turn-on voltage at 1 cd m^{-2}; [f] Maximum luminance; [g] Max current efficiency; [h] Maximum external quantum efficiency; [i] Commission Internationale de l'Eclairage coordinate.

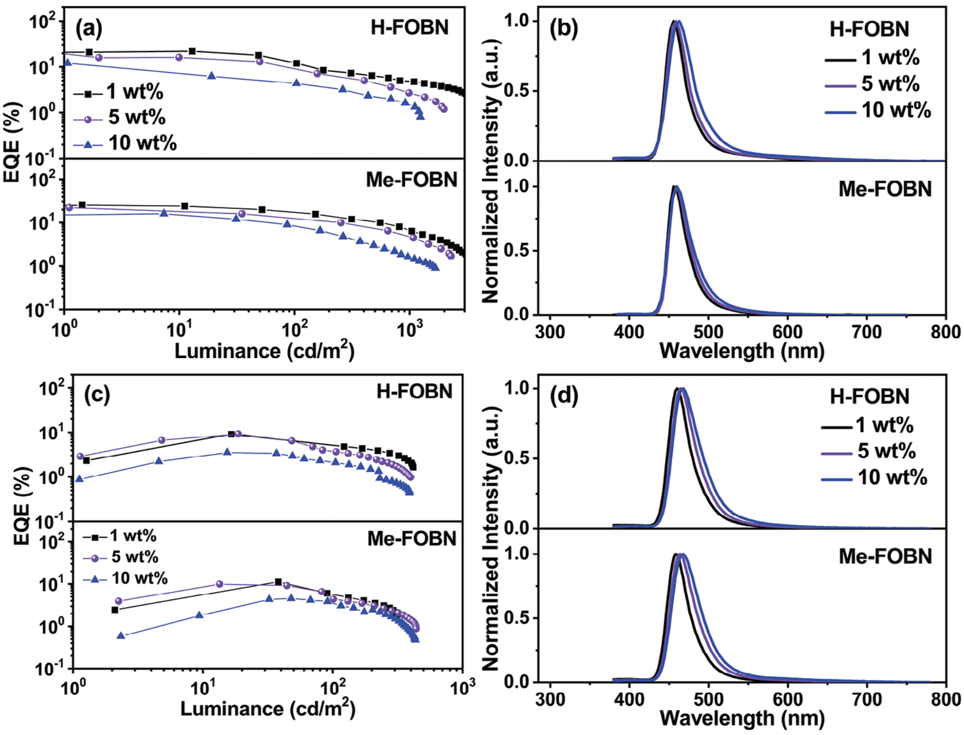

Figure 5. a) EQE-luminance and b) electroluminescence spectra at 1–10 wt% doping concentration of vacuum-deposited OLEDs. c) EQE–luminance and d) electroluminescence spectra at 1–10 wt% doping concentration of solution-processed OLEDs.

intermolecular aggregation of Me-FOBN emitter. The outstanding device performances of pure blue OLEDs based on H-FOBN and Me-FOBN emitters further confirm that the dual-MR-core molecular design strategy is highly effective in developing high efficient MR-TADF emitters.

The L-EQE and EL curves of solution-processed OLEDs of H-FOBN and Me-FOBN emitter at 1 wt% doping concentration were shown in Figure 5c,d. The EL spectra of H-FOBN and Me-FOBN devices have narrowband emission with peaks of 460 nm and 458 nm and small FWHM of 32 nm, respectively, still showing the pure blue emissions with CIE coordinates of (0.14,0.10) and (0.14,0.09). Meanwhile, bathochromic shifting and spectra broadening were also almost negligible as observed at different doping concentrations. The solution-processed OLED devices based on H-FOBN and Me-FOBN emitters provided the display promising EQEs of 9.2% and 11.3%, respectively. Similar, the devices based on Me-FOBN emitter show obvious higher EQE than that of H-FOBN-based devices at all doping concentration, indicating the important role of methyl groups to suppress the intermolecular aggregation. These results may also highlight a new route to achieving the high efficient solution-processable OLEDs in the view of the molecular design of MR-TADF emitter.

3. Conclusion

In conclusion, two novel deep-blue MR-TADF emitters H-FOBN and Me-FOBN were designed and synthesized by employing non-conjugated 9-position substituted fluorene linkages to connect two parent deep-blue N-B-O-skeletons, in which the two emitters possess highly twisted molecular structure and dual-MR-core-emission character. OLEDs based on H-FOBN and Me-FOBN emitters exhibit highly device performance while maintaining the ultrapure deep-blue emission. The vacuum-deposited OLEDs based on Me-FOBN show the excellent EQE of up to 25.1% with small FWHM of 28 nm and CIE of (0.14,0.08), whereas the solution-processed OLEDs based on Me-FOBN also gave a EQE of up to 11.3% with CIE of (0.14,0.09). These promising device performances indicate that the dual-core-strategy provides a feasible method to construct the ultrapure deep-blue MR-TADF emitters with high efficiency.

Supporting Information

Supporting Information is available from the Wiley Online Library or from the author.

Acknowledgements

These authors thank the supports by the National Natural Science Foundation of China (No. 22175049) and the Open Fund of the Key Lab of Organic Optoelectronics & Molecular Engineering, Tsinghua University (No. 53223000122).

Conflict of Interest

The authors declare no conflict of interest.

Data Availability Statement

The data that support the findings of this study are available from the corresponding author upon reasonable request.

Keywords

dual-MR-core, multi-resonance, pure deep blue, solution process, thermally activated delayed fluorescence

Received: June 5, 2024
Revised: August 6, 2024

[1] C. W. Tang, S. A. VanSlyke, *Appl. Phys. Lett.* **1987**, *51*, 913.
[2] S. Chen, Q. Wu, M. Kong, X. Zhao, Z. Yu, P. Jia, W. Huang, *J. Mater. Chem. C* **2013**, *1*, 3508.
[3] Z. Shen, P. E. Burrows, V. Bulović, S. R. Forrest, M. E. Thompson, *Science* **1997**, *276*, 2009.
[4] G. Liu, Z. Li, X. Hu, Y. Qin, C.-S. Lee, D. Chen, L. Wang, J. Liu, P. Wang, Y.-J. Pu, Y. Wang, *Nat. Photonics* **2022**, *16*, 876.
[5] H. Uoyama, K. Goushi, K. Shizu, H. Nomura, C. Adachi, *Nature* **2012**, *492*, 234.
[6] Q. Zhang, J. Li, K. Shizu, S. Huang, S. Hirata, H. Miyazaki, C. Adachi, *J. Am. Chem. Soc.* **2012**, *134*, 14706.
[7] Q. Zhang, B. Li, S. Huang, H. Nomura, H. Tanaka, C. Adachi, *Nat. Photonics* **2014**, *8*, 326.
[8] H. Wang, L. Xie, Q. Peng, L. Meng, Y. Wang, Y. Yi, P. Wang, *Adv. Mater.* **2014**, *26*, 5198.
[9] J. Huang, H. Nie, J. Zeng, Z. Zhuang, S. Gan, Y. Cai, J. Guo, S.-J. Su, Z. Zhao, B. Z. Tang, *Angew. Chem., Int. Ed.* **2017**, *56*, 12971.
[10] A. Endo, K. Sato, K. Yoshimura, T. Kai, A. Kawada, H. Miyazaki, C. Adachi, *Appl. Phys. Lett.* **2011**, *98*, 083302.
[11] M. Lu, X. Song, S. Zou, Y. Zhang, *Chin. J. Lumin.* **2022**, *43*, 1892.
[12] X. Song, Z. Liu, M. Lu, S. Zou, F. Guo, S. Gao, Z. Zhao, B. Z. Tang, Y. Zhang, *J. Mater. Chem. C* **2022**, *10*, 17550.
[13] B. Li, Z. Wang, S.-J. Su, F. Guo, Y. Cao, Y. Zhang, *Adv. Opt. Mater.* **2019**, *7*, 1801496.
[14] X. Dong, S. Shen, Y. Qin, X. Hu, H. Gao, G. Liu, T. Gao, Z. Pang, P. Wang, Y. Wang, *Chin. Chem. Lett.* **2023**, *34*, 108311.
[15] S. S. Song, M. Lu, Y. Wang, Y. Zhang, *Chin. Chem. Lett.* **2024**, *35*, 109118.
[16] Y. Chen, D. Zhang, Y. Zhang, X. Zeng, T. Huang, Z. Liu, G. Li, L. Duan, *Adv. Mater.* **2021**, *33*, 2103293.
[17] Y. Fu, H. Liu, D. Yang, D. Ma, Z. Zhao, B. Z. Tang, *Sci. Adv.* **2021**, *7*, eabj2504.
[18] B. Li, Z. Li, T. Hu, Y. Zhang, Y. Wang, Y. Yi, F. Guo, L. Zhao, *J. Mater. Chem. C* **2018**, *6*, 2351.
[19] N. Takada, T. Tsutsui, S. Saito, *Appl. Phys. Lett.* **1993**, *63*, 2032.
[20] D. Poitras, C.-C. Kuo, C. Py, *Opt. Express* **2008**, *16*, 8003.
[21] F. Santoro, A. Lami, R. Improta, J. Bloino, V. Barone, *J. Chem. Phys.* **2008**, *128*, 224311.
[22] C. Lv, X. Wang, Q. Zhang, Y. Zhang, *Mater. Chem. Front.* **2023**, *7*, 2809.
[23] H. J. Kim, T. Yasuda, *Adv. Opt. Mater.* **2022**, *10*, 2201714.
[24] F.-M. Liu, L.-Y. Ding, Y.-J. Yu, M.-T. Li, L.-S. Liao, Z.-Q. Jiang, *J. Mater. Chem. C* **2023**, *11*, 11425.
[25] X. Song, S. Shen, S. Zou, F. Guo, Y. Wang, S. Gao, Y. Zhang, *Chem. Eng. J.* **2023**, *467*, 143557.
[26] X. Song, S. Shen, S. Zou, Y. Wang, F. Guo, S. Gao, Y. Zhang, *Chem. Eng. J.* **2024**, *481*, 148794.
[27] K. Schmidt, S. Brovelli, V. Coropceanu, J.-L. Brédas, C. Bazzini, T. Caronna, R. Tubino, F. Meinardi, *J. Phys. Chem. A* **2006**, *110*, 11018.
[28] Y. Kondo, K. Yoshiura, S. Kitera, H. Nishi, S. Oda, H. Gotoh, Y. Sasada, M. Yanai, T. Hatakeyama, *Nat. Photonics* **2019**, *13*, 678.
[29] X. Song, S. Shen, S. Zou, F. Y. Guo, S. Y. Gao, Y. Wang, Y. Zhang, *J. Mater. Chem. C* **2023**, *11*, 16928.
[30] I. S. Park, M. Yang, H. Shibata, N. Amanokura, T. Yasuda, *Adv. Mater.* **2022**, *34*, 2107951.
[31] T. Hatakeyama, K. Shiren, K. Nakajima, S. Nomura, S. Nakatsuka, K. Kinoshita, J. Ni, Y. Ono, T. Ikuta, *Adv. Mater.* **2016**, *28*, 2777.
[32] Y. Xu, Z. Cheng, Z. Li, B. Liang, J. Wang, J. Wei, Z. Zhang, Y. Wang, *Adv. Opt. Mater.* **2020**, *8*, 1902142.
[33] M. Yang, I. S. Park, T. Yasuda, *J. Am. Chem. Soc.* **2020**, *142*, 19468.
[34] K. Zhang, X. Wang, Y. Chang, Y. Wu, S. Wang, L. Wang, *Angew. Chem., Int. Ed.* **2023**, *62*, 202313084.
[35] K. R. Naveen, J. H. Oh, H. S. Lee, J. H. Kwon, *Angew. Chem., Int. Ed.* **2023**, *62*, 202306768.
[36] N. Peethani, N. Y. Kwon, C. W. Koh, S. H. Park, J. M. Ha, M. J. Cho, H. Y. Woo, S. Park, D. H. Choi, *Adv. Opt. Mater.* **2024**, *12*, 2301217.
[37] L. Yang, P. Wang, K. Zhang, S. Wang, S. Shao, L. Wang, *Dyes Pigm.* **2023**, *216*, 111371.
[38] Y. Shi, H. Ma, Z. Sun, W. Zhao, G. Sun, Q. Peng, *Angew. Chem., Int. Ed.* **2022**, *61*, 202213463.